First-order route to antiphase clustering in adaptive simplicial complexes

Ajay Deep Kachhvah [*] and Sarika Jalan [†]

Complex Systems Laboratory, Department of Physics, Indian Institute of Technology Indore - Simrol, Indore 453552, India

This Letter investigates the transition to synchronization of oscillator ensembles encoded by simplicial complexes in which pairwise and higher-order coupling weights alter with time through a rate-based adaptive mechanism inspired by the Hebbian learning rule. These simultaneously evolving disparate adaptive coupling weights lead to a phenomenon in that the in-phase synchronization is completely obliterated; instead, the antiphase synchronization is originated. In addition, the onsets of antiphase synchronization and desynchronization are manageable through both dyadic and triadic learning rates. The theoretical validation of these numerical assessments is delineated thoroughly by employing Ott-Antonsen dimensionality reduction. The framework and results of the Letter would help understand the underlying synchronization behavior of a range of real-world systems, such as the brain functions and social systems where interactions evolve with time.

In the past, the inclusion of higher-order interactions has not drawn much attention in investigations of the underlying dynamics influencing distinct processes taking place on a variety of complex systems ranging from physical to biological systems. Nevertheless, many complex systems, such as the brain networks [1,2] and social interaction networks [3,4], have the underlying structure of higher-order connections, which can be exemplified by simplicial complexes [5,6]. These higher-order interactions can be encoded by simplicial complexes, which are sets of n-simplexes, filled cliques of $n + 1$ nodes, viz., vertices (0-simplex), lines (1-simplex), triangles (2-simplex), tetrahedrons (3-simplex), etc. An n-simplicial complex comprises the n-simplexes and the downward closure $(n − 1)$-simplexes. Recently, the call for simplicial complexes in encoding higher-order interactions in complex systems has led to much interest in untangling the reciprocation between network geometry and dynamical processes [7–17]. One phenomenon that naturally arises out of simplicial complex encoded higher-order interactions is the abrupt transition to synchronization and desynchronization [8,11,18]. Simplicial complexes are a suitable candidate for capturing the underlying geometry of complex systems; for instance, they have been used to encode the topological map of the environment's geometrical features captured by the hippocampus [19].

The role of adaptation is instrumental in the growth and proper functioning of many physical and biological systems. For instance, there is a widespread perception in neuroscience that synaptic plasticity among the firing neurons forms the basis for the learning process and memory storage in the brain [20,21]. It was Hebb [22] who first put forth the concept that the simultaneous firing of interacting neurons strengthens the synaptic connectivity between them [21,23,24]. Spike-timing-dependent plasticity between firing neurons is one popular approach to understand the impact of synaptic plasticity on various processes transpiring in the brain [25–27]. Nevertheless, the correlation between presynaptic and postsynaptic spike timings of the interacting neurons is also encoded in phases of the oscillators to realize a neural network with synaptic plasticity. Such rate-based models of synaptic plasticity between the interacting neurons have divulged riveting structures and processes, for instance, cluster synchronization [28–33] and abrupt synchronization and desynchronization [34–38] in monolayer and multilayer networks. In cluster synchronization, a network is segregated into distinct clusters of nodes in which the nodes of the same cluster are mutually synchronized; still, the distinct clusters are not mutually synchronized. A diverse range of real-world systems exists, such as the cortical brain network [39], the power grid network [40], consensus dynamics [41], and schools of fish and swarms of birds [42], having cluster synchronization as a key mechanism of their evolution or functioning. This Letter focuses on the impact of the simultaneous adaptation of different simplex couplings on the transition to synchronization and desynchronization in simplicial complexes. Here, the adaptation of 1-simplex (dyadic) and 2-simplex (triadic) couplings in a simplicial complex are inspired by the Hebbian learning rule, i.e., the dyadic and triadic weights are strengthened (weakened) if the dyad and triad of the oscillators establishing the respective connectivities are in phase (out of phase), respectively. Such a concurrent adaptation in simplicial complexes leads to the fascinating phenomenon of abrupt antiphase synchronization while the in-phase synchronization is completely inhibited. Moreover, the proposed model allows us to determine the onset of synchronization through the learning parameters. The rigorous theoretical analysis provided also validates these numerical findings.

---

*iajaydeep@gmail.com

†Author to whom correspondence should be addressed: sarika@iiti.ac.in

To begin with, the phase evolution of N nondentical Kuramoto oscillators [43] in a simplicial complex under the impression of the rate-based learning of 1-simplex and 2-simplex couplings is given by

$$\dot{\theta}_i = \omega_i + \frac{\lambda_1}{\langle k^{[1]} \rangle} \sum_{j=1}^{N} A_{ij} \sin(\theta_j - \theta_i) + \frac{\lambda_2}{2! \langle k^{[2]} \rangle} \sum_{j,k=1}^{N}$$
$$\times B_{ijk} \sin(2\theta_j - \theta_k - \theta_i), \qquad (1)$$

where $\theta_i(\omega_i)$, $i = 1, \ldots, N$ denotes the instantaneous phases (intrinsic frequencies) of an ith oscillator in the simplicial complex. λ_1 and λ_2 are the coupling strengths of 1-simplex and 2-simplex interactions, respectively. We conserve the global coupling of the 1-simplex and 2-simplex interactions in the complex by setting $\lambda = \lambda_1 + \lambda_2$, irrespective of their topology assimilated in A and B. This choice, for any given λ, allows us to maintain the dominance of one type of simplex interaction over the other type through a propensity parameter $p \in [0, 1]$ such that $\lambda_1 = (1 - p)\lambda = q\lambda$ and $\lambda_2 = p\lambda$. The number of edges or triangles in the complex a node is part of, is defined as 1- or 2-simplex degrees, i.e., $k_i^{[1]} = \sum_{j=1}^{N} A_{ij}$ or $k_i^{[2]} = \frac{1}{2!} \sum_{j,k=1}^{N} B_{ijk}$, respectively. $\langle k^{[1]} \rangle$ and $\langle k^{[2]} \rangle$ denote mean 1- and 2- simplex degrees, respectively. The 1- and 2-simplex coupling interactions are rescaled by the respective mean degrees so as to bring the respective effective connectivities on an equal footing and assist p in tuning the relative strengths of 1- and 2-simplex interactions:

$$\dot{A}_{ij} = \alpha \cos(\theta_j - \theta_i) - \mu A_{ij},$$
$$\dot{B}_{ijk} = \beta \cos(2\theta_j - \theta_k - \theta_i) - \nu B_{ijk}. \qquad (2)$$

We construct a 2-simplicial complex by identifying unique triangles and unique edges closing the triangles from a random 1-simplicial network. The collective phase evolution and weight adaptation of the adaptive 2-simplicial complex are then governed by Eqs. (1) and (2). To capture the formation of m-clusters in the network, we define an m-cluster order parameter $z_m = R_m e^{i\Psi_m} = \frac{1}{N} \sum_{j=1}^{N} e^{im\theta_j}$, $m = 1, 2$, where R_m and Ψ_m are the amplitude and argument, respectively, of the m-cluster order parameter. R_1 quantifies one-cluster synchronization whereas R_2 quantifies two-cluster synchronization [44].

We numerically evolve Eqs. (1) and (2) to capture the microscopic dynamics of 1- and 2-simplex weights and route to synchronization. All the results presented for a random 2-simplicial complex are for $N = 10^3$, $\langle k^{[1]} \rangle = 14$, and $\langle k^{[2]} \rangle = 10$ with uniform randomly drawn natural frequencies $\omega_i \sim U(-\Delta, \Delta)$, where $\Delta = 1$. All the initial 1-simplex (2-simplex) weights are equal and determined by $A_{ij}(0) = 1/L$ [$B_{ijk}(0) = 1/T$], where L (T) are the number of 1-simplex (2-simplex) connections in the complex. At first, λ is adiabatically increased until a large λ and then adiabatically decreased until $\lambda = 0$. The phase and weight dynamics [Eqs. (1) and (2)] are then simultaneously simulated on the 2-simplicial complex and the order parameters are computed for each λ.

First, we discuss the nature of the transition when the dyadic and triadic weights are static, i.e., only Eq. (1) is evolved, taking $A_{ij} = 1$ and $B_{ijk} = 1$ into account. Such static A_{ij} and B_{ijk} lead to a first-order (abrupt) transition to in-phase (single-cluster) synchronization (R_1) with associated
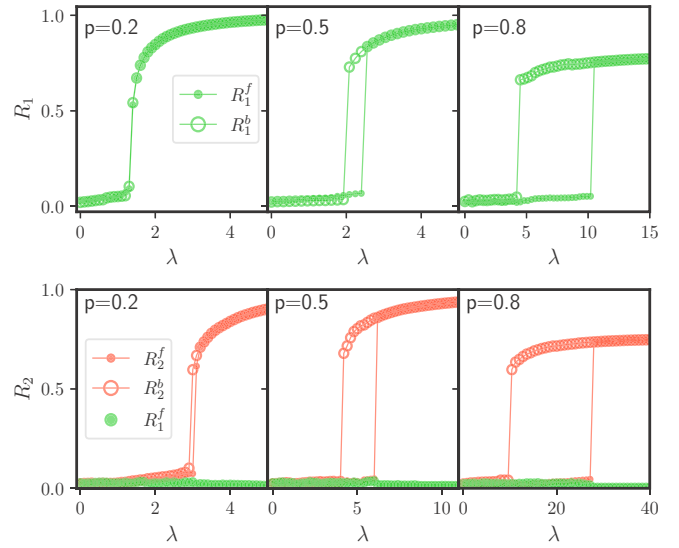

FIG. 1. Antiphase synchronization stems from adaptive couplings: $R_1 - \lambda$ (top row panels) and $R_2 - \lambda$ (bottom row panels) profiles corresponding to the static couplings ($A_{ij} = 1$ and $B_{ijk} = 1$) and the adaptive couplings [Eq. (2)] with learning rates $\alpha = \beta = 1$, respectively, in the random 2-simplicial complex.

hysteresis, as shown in Fig. 1 (top row panels). The dyadic interactions are known to promote synchronization, while the triadic interactions are not. Hence when $p < 0.5$, the dominating dyadic interactions overcome the frustration induced by the triadic ones and lead to synchronization at relatively lower values of λ with a rather reduced hysteresis width. The hysteresis is lost when dyadic interactions are much stronger than the triadic ones for lower values of p. For $p > 0.5$, the triadic interactions dominate, leading to significant frustration, eventually leading to abrupt synchronization at large λ with broader hysteresis. For $p = 1$, however $\lambda_f \to \infty$, as the only interaction type existing among the oscillators, is the triadic one that does not lead to synchronization for any $\lambda > 0$ [8].

Nevertheless, incorporating adaptive 1-simplex and 2-simplex couplings [Eq. (2)] and the phase evolution [Eq. (1)] leads to the finding that the in-phase synchronization (R_1) is completely subsided; instead, a first-order antiphase (two-cluster) synchronization R_2 emanates with an increase in λ [see Fig. 1 (bottom row panels)]. Although the nature of the abrupt R_2 transition for different values of p is analogous to that of the abrupt R_1 transition of the static case, the onset of the abrupt R_2 occurs at relatively larger values of λ than that of R_1. Note that the adaptive pure 2-simplex couplings (when $p = 1$) do not lead to either in-phase or antiphase synchronization with an increase in λ [45], whereas the adaptive pure 1-simplex couplings (when $p = 0$) lead to a second-order antiphase synchronization while in-phase synchronization does not occur [45]. One remarkable feature of the emergent abrupt antiphase (R_2) synchronization and desynchronization is that their respective onsets are entirely manageable through the learning parameters α, β, μ, and ν. Further, the impact of dyadic and triadic learning rates on the characteristics of the R_2 transition is illustrated in Fig. 2. It unveils that the slower learning rates $\alpha = \beta$ prolong the outset of an abrupt transition
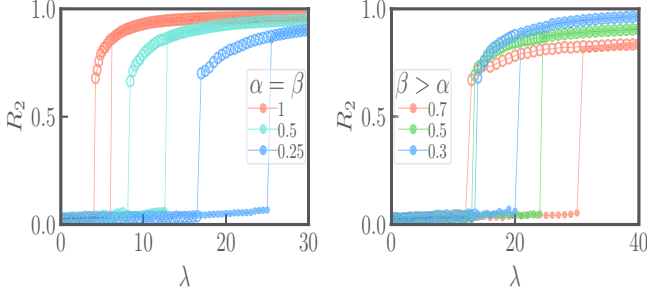
FIG. 2. Slow $\alpha = \beta$ and $\beta > \alpha$ prolong the onset of transition: $R_2 - \lambda$ synchronization profiles for the random 2-simplicial complex with adaptive couplings when $\alpha = \beta \leqslant 1$ and $\beta > \alpha$ (=0.3).

to a higher λ_f. In addition, $\beta > \alpha$ also triggers the abrupt transition at a relatively higher λ_f.

Further, we shed light on the distribution of stationary phases, the adaptive dyadic and triadic weights in the incoherent and coherent states (see left panels of Fig. 3). In the coherent state for $\lambda > \lambda_f$, the stationary A_{ij} (B_{ijk}) are segregated into two clusters. Hence the distribution $P(A_{ij})$ [$P(B_{ijk})$] manifests bimodal peaks at $-\alpha/\mu$ ($-\beta/\nu$) and α/μ (β/ν), with a few A_{ij} and B_{ijk} settling on around 0. The corresponding phases are also set apart into bimodal peaks at a difference of π, thereby $P(\theta_i)$ exhibits antiphase clusters. Nevertheless in the incoherent state for $\lambda < \lambda_f$, $P(A_{ij})$ [$P(B_{ijk})$] follows a beta distribution with peaks at $-\alpha/\mu$ ($-\beta/\nu$) and α/μ (β/ν) and dips at 0 (0). Moreover, $\dot{A}_{ij} = 0$ and $\dot{B}_{ijk} = 0$ yield the dyadic
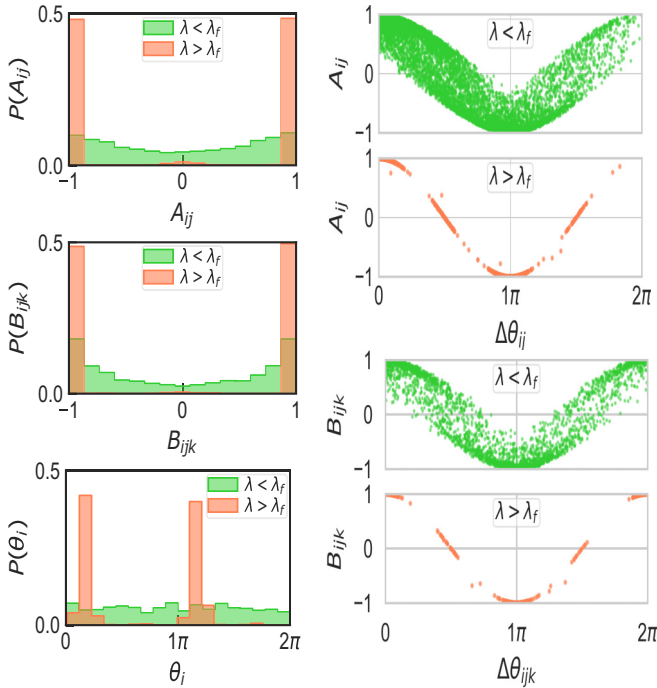

FIG. 3. Steady-state attributes: Distributions $P(A_{ij})$, $P(B_{ijk})$, and $P(\theta_i)$ of the stationary A_{ij}, B_{ijk}, and θ_i, respectively. Also, A_{ij} and B_{ijk} are plotted against $\Delta\theta_{ij}$ and $\Delta\theta_{ijk}$, respectively. All the results are carried out for the random 2-simplicial complex with $\alpha = \beta = 1$ and $\mu = \nu = 1$.

and triadic stationary weights

$$A_{ij} = \frac{\alpha}{\mu}\cos(\Delta\theta_{ij}), \quad B_{ijk} = \frac{\beta}{\nu}\cos(\Delta\theta_{ijk}), \quad (3)$$

where $\Delta\theta_{ij} = (\theta_j - \theta_i)$ and $\Delta\theta_{ijk} = (2\theta_j - \theta_k - \theta_i)$. Equations (3) corroborate the numerical revelations of Fig. 3. In the coherent state, the steady-state extrema $A_{ij} \to \pm\alpha/\mu$ and $B_{ijk} \to \pm\beta/\nu$ correspond to $\Delta\theta_{ij} \to 0, \pi$ and $\Delta\theta_{ijk} \to 0, \pi$, respectively. Also the steady-state $A_{ij} \to 0$ and $B_{ijk} \to 0$ are associated with $\Delta\theta_{ij} \to \pi/2, 3\pi/2$ and $\Delta\theta_{ijk} \to \pi/2, 3\pi/2$, respectively. Nevertheless, in the incoherent state, the uniformly distributed stationary phases require $\Delta\theta_{ij}$ and $\Delta\theta_{ijk}$ to draw the phases from the full range $[0, 2\pi)$. Thereby the stationary A_{ij} and B_{ijk} acquire the weights from the full intervals $[-\alpha/\mu, \alpha/\mu]$ and $[-\beta/\nu, \beta/\nu]$, respectively.

Ott-Antonsen reduction. To seek analytical insight of the underlying higher-order dynamics, we turn our focus to an all-to-all connected 2-simplicial complex modeled as

$$\dot{\theta}_i = \omega_i + \frac{q\lambda}{N}\sum_{j=1}^{N} A_{ij}\sin(\theta_j - \theta_i) + \frac{p\lambda}{N^2}\sum_{j,k=1}^{N} B_{ijk}$$
$$\times \sin(2\theta_j - \theta_k - \theta_i). \quad (4)$$

As per Ott *et al.* [46], the long-time evolution of the order parameter for a system involving adaptive coupling obeys the single differential equation achieved using the Ott-Antonsen ansatz [47] as the precise time dependence of the adaptive coupling would not matter in this analytical treatment. Hence we employ Ott-Antonsen dimensionality reduction to the steady-state collective dynamics of Eqs. (2) and (4). The steady-state collective dynamics can only be achieved when the phases, the dyadic and triadic weights, simultaneously achieve their respective steady states. The evolution of the phases can be described, after plugging into the steady-state expressions for A_{ij} and B_{ijk}, as

$$\dot{\theta}_i = \omega_i + \frac{aq\lambda}{2N}\sum_{j=1}^{N}\sin(2\theta_j - 2\theta_i) + \frac{bp\lambda}{2N^2}\sum_{j,k=1}^{N}$$
$$\times \sin(4\theta_j - 2\theta_k - 2\theta_i), \quad (5)$$

where $a = \alpha/\mu$ and $b = \beta/\nu$. Note that the footprints of both A_{ij} and B_{ijk} are assimilated into Eq. (5) in the form of higher modes of phases in the attractive dyadic and triadic couplings, respectively. The phase evolution can be reexpressed further in terms of the m-cluster order parameters

$$\dot{\theta}_i = \omega_i + \frac{1}{4i}[He^{-2i\theta} - H^*e^{2i\theta}],$$
$$H = aq\lambda z_2 + bp\lambda z_2^* z_4. \quad (6)$$

Considering the system in the continuum limit $N \to \infty$, the collective state of the oscillators at a time t can be delineated by a continuous density function $\rho(\theta, \omega, t)$ such that $\rho(\theta, \omega, t)d\theta d\omega$ denotes the fraction of oscillators with their phases and intrinsic frequencies lying in the ranges of $[\theta, \theta + d\theta]$ and $[\omega, \omega + d\omega]$, respectively. In addition, the density function $\rho(\theta, \omega, t)$ satisfies the normalization condition $\int_0^{2\pi}\rho(\theta, \omega, t)d\theta = 1$ and the continuity equation $\partial_t\rho(\theta, \omega, t) + \partial_\theta[\rho(\theta, \omega, t)\, v(\theta, \omega, t)] = 0$ as the number of oscillators remains conserved. Also, the m-cluster order

parameter can be expressed as $z_m = \iint d\omega d\theta e^{im\theta} \rho(\theta, \omega, t)$. Since $\rho(\theta, \omega, t)$ is a 2π-periodic function with respect to θ, it can be expressed as a Fourier expansion of the form

$$\rho(\theta, \omega, t) = \frac{1}{2\pi}\left[1 + \left\{\sum_{n=1}^{\infty} f_n(\omega, t)e^{in\theta} + \text{c.c.}\right\}\right], \quad (7)$$

where c.c. stands for the complex conjugate of the preceding terms. Ott-Antonsen pointed out that all Fourier coefficients can be classified to Poisson kernels of the form $f_n(\omega, t) = [f(\omega, t)]^n$, where $|f(\omega, t)| \ll 1$ is necessary for the convergence of the series. After plugging into the expressions for $v = \dot{\theta}$ [Eq. (6)] and $f(\theta, \omega, t)$ [Eq. (7)], all Fourier modes then reduce to the same constraint for f, satisfying the single complex-valued differential equation

$$\frac{\partial f^2}{\partial t} + 2i\omega f^2 + \frac{1}{2}[Hf^4 - H^*] = 0, \quad (8)$$

$$z_m = \mathcal{G}f^{*m} = \int_{-\infty}^{\infty} d\omega g(\omega)f^{*m}(\omega, t), \quad m = 2, 4, \quad (9)$$

where the integral operator $\mathcal{G} \equiv \int_{-\infty}^{\infty} d\omega g(\omega)$.

Stability of the incoherent state. The trivial solution $f(\omega, t) = 0$ always exists for Eq. (8) that corresponds to an incoherent state $\rho(\theta, \omega, t) = \frac{1}{2\pi}$ in Eq. (7). Linearizing Eq. (8) around $f(\omega, t) = 0$, we obtain the following linear equation for the perturbed density $\eta(\omega, t)$:

$$\frac{\partial \eta^2}{\partial t} + 2i\omega\eta^2 = \frac{aq\lambda}{2}\mathcal{G}\eta^2. \quad (10)$$

Let γ be the eigenvalues of Eq. (10) such that $\eta(\omega, t) = \eta_0(\omega) e^{\gamma t}$. Then, employing the integral operator $\mathcal{G}$ on both sides of Eq. (10) reduces it to

$$\frac{1}{\lambda} = \frac{aq}{4}\int_{-\infty}^{\infty} d\omega \frac{g(\omega)}{\gamma + i\omega}. \quad (11)$$

Since $\text{Re}[\gamma] = 0$ at the critical coupling strength $\lambda = \lambda_f$, the incoherent state loses stability for $\gamma = 0 + \epsilon' + iy$, where $0 < \epsilon' \ll 1$. Equation (11) now reads as

$$\frac{1}{\lambda} = \frac{aq}{4}\lim_{\epsilon' \to 0}\int_{-\infty}^{\infty} d\omega \frac{g(\omega)}{\epsilon' + i\omega + iy}. \quad (12)$$

Solving Eq. (12) for $g(\omega) = \frac{\Delta}{\pi[\omega^2 + \Delta^2]}$ results in

$$\lambda_f = \frac{4\Delta}{aq} = \frac{4\mu\Delta}{\alpha(1-p)}. \quad (13)$$

Equation (13) unveils that the transition to synchronization is solely caused by the presence of dyadic interactions through parameter p and dyadic rates α and μ and the triadic interactions do not play any role in the onset of synchronization. Also, $p = 1$ yields $\lambda_f \to \infty$, i.e., the incoherence does not lose stability for any $\lambda > 0$ [45].

Solution of coherence. The evolution of the order parameter R_2 can be worked out for a Lorentzian distribution with mean ω_0 and half width Δ, i.e., $g(\omega) = \frac{\Delta}{\pi[(\omega-\omega_0)^2 + \Delta^2]}$. The order parameter in Eq. (8) can be derived using Cauchy's residue theorem by closing the contour to an infinite-radius semicircle in the negative-half complex ω plane, resulting in $z_2 = f^{*2}(\omega_0 - i\Delta, t)$ and $z_4 = f^{*4}(\omega_0 - i\Delta, t) = z_2^2$. Next,
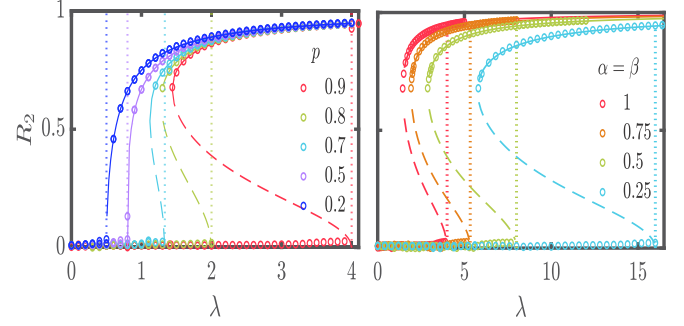

FIG. 4. Analytical vs numerical corroboration of R_2: $R_2 - \lambda$ profiles of the all-to-all connected 2-simplicial complex simulated for Lorentzian $g(\omega)$ with $\Delta = 0.1$, $N = 10^4$, $\mu = 1$, $\nu = 1$. Left panel: Different values of p when $\alpha = \beta = 1$. Right panel: Different values of $\alpha = \beta$ when $p = 0.9$. The solid and dashed lines are the respective theoretical traces of R_2^+ (stable) and R_2^- (unstable) solutions obtained using Eq. (18). The dotted lines are analytical predictions [Eq. (13)] of λ_f.

assessing Eq. (8) at $\omega = \omega_0 - i\Delta$ and then taking a complex conjugate, one gets

$$2\dot{z}_2 - 4i\omega_0 z_2 + 4\Delta z_2 + \lambda z_2^2[aqz_2^* + bpz_2z_4^*] - \lambda[aqz_2 + bpz_2^*z_4] = 0. \quad (14)$$

Next, inserting $z_2 = R_2 e^{i\Psi_2}$ and then equating the real and imaginary parts on both sides of the equation gives

$$2\dot{R}_2 + 4\Delta R_2 + \lambda R_2(R_2^2 - 1)(aq + bpR_2^2) = 0, \quad (15)$$

$$\dot{\Psi}_2 = 2\omega_0. \quad (16)$$

Hence the dynamics of R_2 and Ψ_2 are decoupled. Ψ_2 constantly evolves and is equal to twice the mean of $g(\omega)$. The steady-state evolution of Eq. (15) yields an equation that is cubic in R_2. Thus, $R_2 = 0$ is always an equilibrium whose stability is not affected by the presence of a higher-order interaction. The nonlinear terms stemming from the higher-order interaction in

$$\frac{4\Delta}{\lambda} = -bpR_2^4 + (bp - aq)R_2^2 + aq \quad (17)$$

may give rise to one or two synchronous solutions with the following positive roots for R_2,

$$R_2^{\pm} = \sqrt{\frac{bp - aq \pm \sqrt{(bp - aq)^2 + 4bp(aq - \frac{4\Delta}{\lambda})}}{2bp}}. \quad (18)$$

R_2^+ (R_2^-) represents a stable (an unstable) branch of a synchronous state. The validation of analytical predictions for the order parameter R_2 [Eq. (18)] with its numerical estimations for different sets of parameters is presented in Fig. 4. In the case of a forward transition, in the incoherent state $R_2 = 0$ until $\lambda = \lambda_f = \frac{4\Delta}{aq}$ is reached. At $\lambda = \lambda_f$, R_2 abruptly jumps to $R_2^+(\lambda_f) = \sqrt{1 - \frac{aq}{bp}}$ [while $R_2^-(\lambda_f) = 0$] and the incoherent state ($R_2 = 0$) loses its stability through subcritical pitchfork bifurcation. Nevertheless, for the set of parameters $\{a, b, p\}$ for which $R_2^+(\lambda_f) = \sqrt{1 - \frac{aq}{bp}} = 0$ at $\lambda = \lambda_f$, the incoherent
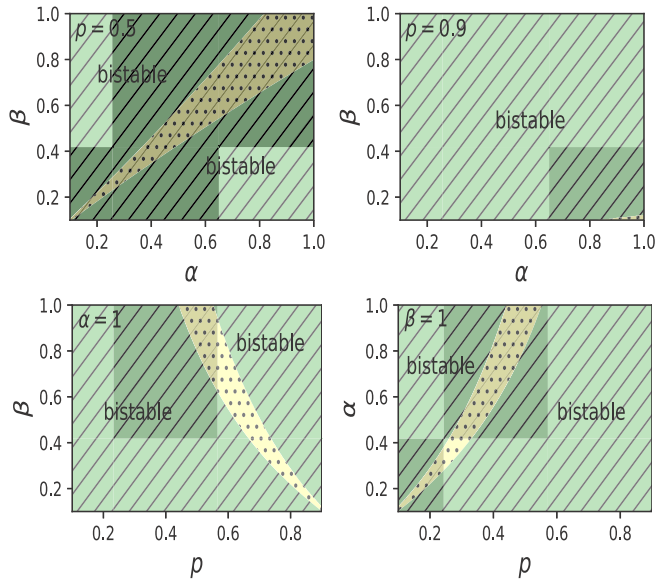
FIG. 5. Bistability domains: Phase diagrams in the $(\alpha - \beta)$, $(p - \alpha)$, and $(p - \beta)$ planes depicting the regions of bistability for the all-to-all connected 2-simplicial complex simulated for Lorentzian $g(\omega)$; $\Delta = 0.1$, $N = 10^3$, $\mu = 1$, and $\nu = 1$. The dotted region manifests nonbistability.

state ($R_2 = 0$) loses its stability through supercritical pitchfork bifurcation and the transition to synchronization takes place via a second-order route.

In the case of a backward transition, R_2^- (saddle point) and R_2^+ (node point) exist in the hysteresis region. As soon as the backward critical coupling strength $\lambda = \lambda_b$ is reached, R_2^+ and R_2^- collide and annihilate each other through saddle-node bifurcation. Thus the stability of the coherent state is totally destroyed and the only remaining solution is $R_2 = 0$. Hence the constraint $d\lambda/dR_2 = 0$ is satisfied at $\lambda = \lambda_b$, which leads to $R_2(\lambda_b) = \sqrt{\frac{1}{2}(1 - \frac{aq}{bp})}$ from Eq. (17). Substituting the value of R_2 back into Eq. (17) supplies us with

$$\lambda_b = \frac{16\Delta bp}{[aq + bp]^2} = \frac{16\Delta p\beta\nu\mu^2}{[\alpha\nu(1 - p) + \beta\mu p]^2}. \tag{19}$$

For that matter, the outset of abrupt desynchronization is characterized by both the dyadic and triadic learning rates.

In Fig. 5, we provide a broad picture of the regions of bistability and nonbistability stretched over the $(\alpha - \beta)$, $(p - \alpha)$, and $(p - \beta)$ planes [48]. The regions illustrated by the slanted green lines represent the bistability region. $aq \neq bp$ and $aq < bp$ are necessary for the existence of bistable solutions exhibiting a hysteresis. The yellow dotted region depicts the nonbistable region corresponding to $aq = bp$ [49]. For $aq = bp$, Eqs. (13) and (19) give $\lambda_f = \lambda_b$, $R_2^+(\lambda_f) = 0$, and $R_2(\lambda_b) = 0$, which conform to a second-order transition to synchronization.

Conclusion. In this Letter, the nature of the transition to synchronization is explored on 2-simplicial complexes where the triadic couplings and the downward closing dyadic couplings evolve in time according to the respective rate-based plasticity inspired by the Hebbian learning rule. Strikingly, such coevolving dyadic and triadic couplings completely diminish single-cluster synchronization and instead trigger two-cluster synchronization in simplicial complexes. It is unveiled that the onset of antiphase synchronization only depends on the dyadic interaction (learning rate) and the higher-order interaction does not play a role. On the other hand, both dyadic and triadic interactions (learning rates) affect the onset of antiphase desynchronization. Further, the numerical findings related to the antiphase order parameter and the forward and backward critical transition points have been validated with the respective analytical predictions by employing the Ott-Antonsen ansatz. It is also shown that the steady dyadic (triadic) weights in the synchronous state form two clusters of equal and opposite magnitudes along the lines of the oscillators forming the antiphase clusters.

The simplicial structures involving the simultaneous adaptation of pairwise and higher-order interactions would help elucidate the underlying mechanism of cluster formation in the brain functional networks, such as antiphase patterns in the cortical neural network.

[1] G. Petri, P. Expert, F. Turkheimer, R. Carhart-Harris, D. Nutt, P. J. Hellyer, and F. Vaccarino, Homological scaffolds of brain functional networks, J. R. Soc. Interface **11**, 20140873 (2014).

[2] A. R. Benson, R. Abebe, M. T. Schaub, A. Jadbabaie, and J. Kleinberg, Simplicial closure and higher-order link prediction, Proc. Natl. Acad. Sci. U.S.A. **115**, 11221 (2018).

[3] I. Iacopini, G. Petri, A. Barrat, and V. Latora, Simplicial models of social contagion, Nat. Commun. **10**, 2485 (2019).

[4] J. T. Matamalas, S. Gómez, and A. Arenas, Abrupt phase transition of epidemic spreading in simplicial complexes, Phys. Rev. Research **2**, 012049(R) (2020).

[5] V. Salnikov, D. Cassese, and R. Lambiotte, Simplicial complexes and complex systems, Eur. J. Phys. **40**, 014001 (2019).

[6] J. H. C. Whitehead, Simplicial spaces, nuclei and *m*-groups, Proc. London Math. Soc. **s2-45**, 243 (1939).

[7] T. Tanaka and T. Aoyagi, Multistable Attractors in a Network of Phase Oscillators with Three-Body Interactions, Phys. Rev. Lett. **106**, 224101 (2011).

[8] P. S. Skardal and A. Arenas, Abrupt Desynchronization and Extensive Multistability in Globally Coupled Oscillator Simplexes, Phys. Rev. Lett. **122**, 248301 (2019).

[9] C. Xu, X. Wang, and P. S. Skardal, Bifurcation analysis and structural stability of simplicial oscillator populations, Phys. Rev. Research **2**, 023281 (2020).

[10] A. P. Millán, J. J. Torres, and G. Bianconi, Explosive Higher-Order Kuramoto Dynamics on Simplicial Complexes, Phys. Rev. Lett. **124**, 218301 (2020).

[11] P. S. Skardal and A. Arenas, Higher order interactions in complex networks of phase oscillators promote abrupt synchronization switching, Commun. Phys. **3**, 218 (2020).

[12] M. Lucas, G. Cencetti, and F. Battiston, Multiorder Laplacian for synchronization in higher-order networks, Phys. Rev. Research **2**, 033410 (2020).

[13] F. Battiston, G. Cencetti, I. Iacopini, V. Latora, M. Lucas, A. Patania, J.-G. Young, and G. Petri, Networks beyond pairwise interactions: Structure and dynamics, Phys. Rep. **874**, 1 (2020).

[14] R. Ghorbanchian, J. G. Restrepo, J. J. Torres, and G. Bianconi, Higher-order simplicial synchronization of coupled topological signals, Commun. Phys. **4**, 120 (2021).

[15] C. Xu and P. S. Skardal, Spectrum of extensive multiclusters in the Kuramoto model with higher-order interactions, Phys. Rev. Research **3**, 013013 (2021).

[16] M. Chutani, B. Tadić, and N. Gupte, Hysteresis and synchronization processes of Kuramoto oscillators on high-dimensional simplicial complexes with competing simplex-encoded couplings, Phys. Rev. E **104**, 034206 (2021).

[17] H. Sun and G. Bianconi, Higher-order percolation processes on multiplex hypergraphs, Phys. Rev. E **104**, 034306 (2021).

[18] C. Kuehn and C. Bick, A universal route to explosive phenomena, Sci. Adv. **7**, eabe3824 (2021).

[19] Y. Dabaghian, F. Mémoli, L. Frank, and G. Carlsson, A topological paradigm for hippocampal spatial map formation using persistent homology, PLoS Comput. Biol. **8**, e1002581 (2012).

[20] E. Shimizu, Y. P. Tang, C. Rampon, and J. Z. Tsien, NMDA receptor-dependent synaptic reinforcement as a crucial process for memory consolidation, Science **290**, 1170 (2000).

[21] L. F. Abbott and S. B. Nelson, Synaptic plasticity: taming the beast, Nat. Neurosci. **3**, 1178 (2000).

[22] D. O. Hebb, *The Organization of Behavior* (Wiley, New York, 1949).

[23] H. Markram, J. Lübke, M. Frotscher, and B. Sakmann, Regulation of synaptic efficacy by coincidence of postsynaptic APs and EPSPs, Science **275**, 213 (1997).

[24] L. I. Zhang, H. W. Tao, C. E. Holt, W. A. Harris, and M. Poo, A critical window for cooperation and competition among developing retinotectal synapses, Nature (London) **395**, 37 (1998).

[25] V. P. Zhigulin, M. I. Rabinovich, R. Huerta, and H. D. I. Abarbanel, Robustness and enhancement of neural synchronization by activity-dependent coupling, Phys. Rev. E **67**, 021901 (2003).

[26] A. Knoblauch, F. Hauser, M.-O. Gewaltig, E. Körner, and G. Palm, Does spike-timing-dependent synaptic plasticity couple or decouple neurons firing in synchrony? Front. Comput. Neurosci. **6**, 55 (2012).

[27] J. Zirkle, and L. L. Rubchinsky, Spike-timing dependent plasticity effect on the temporal patterning of neural synchronization, Front. Comput. Neurosci. **14**, 52 (2020).

[28] R. K. Niyogi and L. Q. English, Learning-rate-dependent clustering and self-development in a network of coupled phase oscillators, Phys. Rev. E **80**, 066213 (2009).

[29] T. Aoki and T. Aoyagi, Co-evolution of Phases and Connection Strengths in a Network of Phase Oscillators, Phys. Rev. Lett. **102**, 034101 (2009).

[30] R. Gutiérrez, A. Amann, S. Assenza, J. Gómez-Gardeñes, V. Latora, and S. Boccaletti, Emerging Meso- and Macroscales from Synchronization of Adaptive Networks, Phys. Rev. Lett. **107**, 234103 (2011).

[31] E. Pitsik, V. Makarov, D. Kirsanov, N. Frolov, M. Goremyko, X. Li, Z. Wang, A. Hramov, and S. Boccaletti, Inter-layer competition in adaptive multiplex network, New J. Phys. **20**, 075004 (2018).

[32] P. Khanra, S. Ghosh, K. Alfaro-Bittner, P. Kundu, S. Boccaletti, C. Hens, and P. Pal, Identifying symmetries and predicting cluster synchronization in complex networks, Chaos, Solitons Fractals **155**, 111703 (2022).

[33] I. Shepelev, A. Bukh, G. Strelkova, and V. Anishchenko, Anti-phase relay synchronization of wave structures in a heterogeneous multiplex network of 2D lattices, Chaos, Solitons Fractals **143**, 110545 (2021).

[34] V. Avalos-Gaytán, J. A. Almendral, I. Leyva, F. Battiston, V. Nicosia, V. Latora, and S. Boccaletti, Emergent explosive synchronization in adaptive complex networks, Phys. Rev. E **97**, 042301 (2018).

[35] A. D. Kachhvah, X. Dai, S. Boccaletti, and S Jalan, Interlayer Hebbian plasticity induces first-order transition in multiplex networks, New J. Phys. **22**, 122001 (2020).

[36] N. Frolov and A. Hramov, Coexistence of interdependence and competition in adaptive multilayer network, Chaos, Solitons Fractals **147**, 110955 (2021).

[37] R. Berner, S. Vock, E. Schöll, and S. Yanchuk, Desynchronization Transitions in Adaptive Networks, Phys. Rev. Lett. **126**, 028301 (2021).

[38] S. Majhi, M. Perc, and D. Ghosh, Dynamics on higher-order networks: a review, J. R. Soc. Interface **19**, 20220043 (2022).

[39] M. Lodi, F. D. Rossa, F. Sorrentino, and M. Storace, Analyzing synchronized clusters in neuron networks, Sci. Rep. **10**, 16336 (2020).

[40] L. M. Pecora, F. Sorrentino, A. M. Hagerstrom, T. E. Murphy, and R. Roy, Cluster synchronization and isolated desynchronization in complex networks with symmetries, Nat. Commun. **5**, 4079 (2014).

[41] M. T. Schaub, N. O'Clery, Y. N. Billeh, J.-C. Delvenne, R. Lambiotte, and M. Barahona, Graph partitions and cluster synchronization in networks of oscillators, Chaos **26**, 094821 (2016).

[42] C. K. Hemelrijk and H. Hildenbrandt, Schools of fish and flocks of birds: their shape and internal structure by self-organization, Interface Focus **2**, 726 (2012).

[43] Y. Kuramoto, Self-entrainment of a population of coupled nonlinear oscillators, in *International Symposium on Mathematical Problems in Theoretical Physics*, edited by H. Araki, Lecture Notes in Physics, Vol. 39 (Springer, Berlin, 1975), pp. 420–422.

[44] H. Daido, Multibranch Entrainment and Scaling in Large Populations of Coupled Oscillators, Phys. Rev. Lett. **77**, 1406 (1996).

[45] A. D. Kachhvah and S. Jalan, Hebbian plasticity rules abrupt desynchronization in pure simplicial complexes, New J. Phys. **24**, 052002 (2022).

[46] E. Ott and T. M. Antonsen, Long time evolution of phase oscillator systems, Chaos **19**, 023117 (2009).

[47] E. Ott and T. M. Antonsen, Low dimensional behavior of large systems of globally coupled oscillators, Chaos **18**, 037113 (2008).

[48] See Supplemental Material at http://link.aps.org/supplemental/10.1103/PhysRevE.105.L062203 for details concerning the stationary dyadic and triadic weights, and alternative bistability phase diagrams.

[49] The nonbistable region also includes the set of parameters yielding hysteresis width tending to zero, i.e., $|\lambda_f - \lambda_b| < 0.01$.